

Development of a high-throughput microscale cell disruption platform for *Pichia pastoris* in rapid bioprocess design

Benjamin A. F. Bláha¹, Stephen A. Morris^{1,2}, Olotu W. Ogonah¹, Vincenzo Crescente², William Rosenberg², Sophie Maucourant² and Tarit K. Mukhopadhyay¹

Running title: High-throughput microscale cell disruption platform for Pichia pastoris

1: The Advanced Centre for Biochemical Engineering, Department of Biochemical Engineering, University College London, Bernard Katz Building, Gordon Street, London, WC1E 7JE, UK; telephone: +44 (0)20 7679 0438; fax: +44 (0)20 7916 3943; e-mail: ucbetkm@ucl.ac.uk

2: IQur Limited, London Bioscience Innovation Centre, 2 Royal College Street, London, NW1 0NH, UK; telephone +44 (0)20 7691 1122

Correspondence to: Tarit K. Mukhopadhyay

This article has been accepted for publication and undergone full peer review but has not been through the copyediting, typesetting, pagination and proofreading process which may lead to differences between this version and the Version of Record. Please cite this article as doi: 10.1002/btpr.2555

© 2017 American Institute of Chemical Engineers Biotechnol Prog
Received: Jun 06, 2017; Revised: Jul 28, 2017; Accepted: Aug 27, 2017

Abstract

The time and cost benefits of miniaturized fermentation platforms can only be gained by employing complementary techniques facilitating high-throughput at small sample volumes.

Microbial cell disruption is a major bottleneck in experimental throughput and is often restricted to large processing volumes. Moreover, for rigid yeast species such as *Pichia pastoris*, no effective high-throughput disruption methods exist.

This study describes the development of an automated, miniaturized, high-throughput, non-contact, scalable platform based on Adaptive Focused Acoustics (AFA) to disrupt *P. pastoris* and recover intracellular heterologous protein.

Augmented modes of AFA were established by investigating vessel designs and a novel enzymatic pre-treatment step. Three different modes of AFA were studied and compared to the performance high pressure homogenization. For each of these modes of cell disruption, response models were developed to account for five different performance criteria. Using multiple responses not only demonstrated that different operating parameters are required for different response optima, with highest product purity requiring suboptimal values for other criteria, but also allowed for AFA-based methods to mimic large-scale homogenization processes.

These results demonstrate that AFA-mediated cell disruption can be used for a wide range of applications including buffer development, strain selection, fermentation process development and whole bioprocess integration.

Keywords

Pichia pastoris, scale-down, high-throughput, Adaptive Focused Acoustics, cell disruption, homogenization

Introduction

Scale-down bioprocesses form the backbone of rapid bioprocess design, allowing for cost-effective and rapid development of biopharmaceutical production processes. Specifically, small-scale fermentation process design combined with multivariate data analysis techniques and subsequent process up-scaling has proven to be effective for characterizing and optimizing industrial-scale operations¹⁻⁴.

Pichia pastoris, recently reassigned to the genus *Komagataella*, is a methanol assimilating yeast that has been receiving increased industrial attention over the past two decades due to its potential to produce a wide array of complex biopharmaceuticals⁵⁻¹².

P. pastoris offers the potential of heterologous protein secretion, however depending on physical and chemical properties of the protein of interest, this is not always a viable option^{13,14}. In this alternative scenario, the product of interest needs to be liberated from the interior of the cell through a disruption process.

A widely-used method of cell disruption in microbial bioprocessing is High Pressure Homogenization (HPH). This method involves passing a cell suspension at high pressure, and often low temperature to mitigate heat effects, through an adjustable valve with a restricted cavity. Through high velocity impact, cavitation, fluid shear and decompression the cells are disrupted causing their contents to be released in the media. This process can be repeated for several passes increasing the levels of cell disruption and debris generated^{15,16}. Overall cell disruption can be described with the following equation¹⁷:

$$\ln\left(\frac{R_{max}}{R_{max}-R}\right) = kNp^\alpha \quad (1)$$

Where, R_{max} is the maximum amount of releasable protein, R the observed amount of released protein, N the discrete number of passes through the valve, k a temperature dependent rate constant and is specific to the organism being disrupted; p the operating pressure and α is a measure of a microbe's resistance to disruption. In addition, efficiency of homogenization is

known to decrease at high biomass suspension concentrations¹⁸. Therefore, for a given organism harvested at fixed conditions the following relation can be observed for cell disruption:

$$R = f(N, p, [X]) \quad (2)$$

Where $[X]$ is the concentration of biomass in suspension.

However, high pressure homogenization is only suitable for processing large volumes with the smallest representative size being 40mL using an APV Gaulin Lab40 homogenizer¹⁹.

Scale-down bioprocess sequences often start with the use of microtiter plates or miniaturized bioreactors^{20,21}. HPH therefore remains an incompatible platform for scale-down bioprocesses, as sample volumes are often in the microliter range.

Small-scale cell disruption of yeasts has often been achieved using bead lysis methods²².

However limitations of bead-mediated lysis include the requirement of additional process bottlenecks demanding the removal of beads from lysate, poor temperature control, lower process reproducibility due to a requirement of bead size uniformity, loss of product due to residual volume after sample processing and high surface-to-volume ratios which could lead to adhesion of cellular material²³.

Adaptive Focused Acoustics (AFA) has shown to be a suitable miniaturized platform for the disruption of the yeast, *Saccharomyces cerevisiae*²⁴. An AFA device generates acoustic shock waves in the kilohertz (KHz) region. These sonic waves cause controlled cavitation at a focal point within the sample vessel²⁵. The device can process up to 12-96 samples in a batch, enabling rapid, high-throughput, non-contact cell disruption. Figure 1 explains the operating parameters associated with the Covaris E210. Process variables contributing to cell disruption can be described as follows:

$$R = f(DF, I, cpb, t, [X]) \quad (3)$$

Duty Factor, DF (%), refers to the relative time between sonic bursts, hence

$$DF = (t_1/t_2) \cdot 100. \quad (4)$$

Intensity, I (mV), denotes the amplitude of the sonic wave. Cycles per burst, cpb , refers to the amount of cycles per acoustic wave. Time, t (s), refers to the total acoustic exposure time. $[X]$ (g/L) refers to the wet cell biomass concentration in suspension. Although there are studies showing promising results for extracting intracellular product from *S. cerevisiae*, no extensive studies exist for AFA-mediated cell disruption of *P. pastoris*.

This study examined AFA-mediated cell disruption of *P.pastoris* (KM71h) with the Covaris E210 series to liberate Tandem Core Hepatitis B core Virus-Like Particles (TC-HBc VLPs) described by ²⁶. After screening for significant factors, three AFA experiments were performed to generate Response Surface Models (RSMs) to account for changes in vessel design and enzymatic pre-treatment of samples. This data was subsequently compared to large-scale performance by generating RSMs for HPH-based cell disruption.

To choose appropriate responses to generate RSMs, performance criteria had to be defined. Most studies have only defined total soluble protein content as a performance criteria of cell disruption processes. However, maximizing cell disruption is not always the main objective of cell disruption. This study has outlined data with five different performance criteria and generated RSMs for each criterion, for each experiment: (1) Total cell disruption, measured as the concentration of total soluble protein, R (mg/mL), (2) specific cell disruption, defined as the amount of protein released per unit of suspended biomass, R_s (mg/g_{WCW}), (3) total product recovery expressed as the concentration of soluble Tandem Core Hepatitis B core protein $[TC-HBc]$ ($\mu g/mL$), (4) specific product recovery, $TC-HBc_s$ ($\mu g/g_{WCW}$) and (5) product purity, expressed as a ratio of total recover product relative to the amount of total release soluble protein, P (%). By understanding the response models of multiple performance criteria, this study aimed to broaden the range applications of AFA-mediated cell disruption as well as create a performance-based scaling method for cell disruption.

Materials and Methods

All chemical and reagents were purchased from Sigma-Aldrich (Gillingham, UK) unless stated otherwise.

Process Overview

Figure 2 depicts a summary of the unit operations involved in experimental methods in this series of studies. Note that only unit operations “C” were varied in this study. The responses (R , R_s , $[TC-HBc]$, $TC-HBc_s$, P) of these variations were measured after the second centrifugation step post lysis, “E”. Material for further qualitative analysis was fractioned prior to unit operation “D”.

***Pichia pastoris* Cell Engineering and Fermentation**

A transformed *Pichia pastoris* strain of the Mut^S phenotype (KM71h) was provided by iQur Ltd, (London, UK). Upon induction, this strain expressed Tandem Core HBc protein with single lysine amino acids inserts displayed on its two insertion regions.

Invitrogen’s fermentation protocol²⁷ for *Pichia pastoris* Mut^S strains was used to generate experimental material in a 30L BIOSTAT Cplus bioreactor (Sartorius Stedim, Epsom UK).

The reactor was filled with 11.5L Basal Salts Medium to achieve a total starting working volume of 12L post-inoculation. Details of this procedure are described below.

For seed culture, 2 x 250mL of Buffer Glycerol-complex BMGY medium²⁸ was inoculated with 1.8 mL cell bank culture [BMGY culture, 30%vol glycerol, optical density $A_{600nm}=25.0$] in 2L baffled Nalgene® shakeflasks. After 16 hours, the absorbance at 600nm of the seed culture was 20-30 relative absorbance units. A variable fraction of the culture was centrifuged at 3200 g, 20°C, 10 min and resuspended in 500mL Basal Salts Medium to achieve defined conditions and a starting bioreactor inoculation optical density of 1 absorbance unit at 600nm.

The bioreactor was run in batch-mode after inoculation. The Dissolved Oxygen Tension (DOT) setpoint was set at 30% and was controlled in a sequence cascade by agitating the impeller between 468 to 1123 rpm followed by oxygen gas blending in ratio mode at a constant volumetric gas flowrate of 0.25vvm. pH range was maintained between 4.75-5.0 and pre-induction temperature at $30\pm 0.1^\circ\text{C}$. A 20% drop in Carbon Evolution Rate (CER) and spike in DOT, indicating depletion of carbon source, triggered a fed-batch glycerol feed. This was generally observed between 18-20 hours after bioreactor inoculation. This glycerol fed-batch phase was maintained for a fixed 4 hours at a constant flow rate of 18.15 milliliters per liter initial working volume per hour ($\text{mL}/L_i/\text{h}$). 20 minutes prior to the induction phase the temperature setpoint was adjusted to 25°C . The end of the glycerol fed-batch phase triggered the methanol induction phase. For the first two hours of the induction phase the methanol flow rate was kept constant at $1\text{mL}/L_i/\text{h}$. After this the feed rate was increased by 10% increments every 30 minutes until a target feed rate of $5.5\text{mL}/L_i/\text{h}$ was reached.

After 40 hours of induction the culture was cooled to 12°C to minimize proteolytic activity. Fermentation broth was harvested at 3000 g, 20 min and 4°C . The wet pellets were weighed and stored at -20°C .

Cell Disruption and Primary Recovery

Lysis Reagents

MOPS lysis buffer: 50mM 3-(N-morpholino)propanesulfonic acid (MOPS), (1mM 4-(2-aminoethyl) benzenesulfonyl fluoride (AEBSF) hydrochloride, 5U/mL benzonase (Cat. No. E8263-25KU), 5mM dithiothreitol (DTT) in reverse osmosis water titrated with 1M sodium hydroxide to achieve a of pH 7.5 (at 10°C). EDTA stock solution: 500mM Ethylenediaminetetraacetic acid tri-sodium salt in RO water. Triton-X100 stock solution: 10% vol. Triton-X100 in RO water. Lyticase stock solution: 2000U/mL lyticase from *Arthrobacter luteus* (Cat. No. L2524), 100mM potassium phosphate, 100mM sodium

hydroxide, 50% vol. glycerol, pH 7.5 in RO water. MOPS Enzymatic lysis buffer: 4% vol. lyticase stock solution and 1% vol. Triton-X100 stock solution in MOPS lysis buffer.

High Pressure Homogenization Optimization

Frozen cell paste was weighed and resuspended in lysis buffer to achieve wet cell weight (WCW) concentrations of 50, 75 and 100 g/L. 40mL aliquots were prepared and subsequently disrupted using a APV Gaulin Lab40 high pressure homogenizer at 300, 750 and 1200 bar, for 1, 3 and 5 passes. Homogenization was performed at $T < 10^{\circ}\text{C}$ with the aid of a glycol cooling loop.

To each homogenized sample a 1% volumetric addition of Triton X-100 stock solution was added to facilitate protein release. After a one-hour incubation period at 4°C a 1% volumetric addition of EDTA stock solution was added to each aliquot. 1 mL from each aliquot was collected for clarification and subsequent analysis.

Adaptive Focused Acoustics Characterization

The Covaris E210 was used to perform AFA-mediated cell disruption. Experiments were conducted with 1mL cell suspensions in MOPS lysis buffer, 0.1% Triton X-100, in 12 x 12mm milliTUBE vials, each containing an integrated fiber to assist disruption. The tubes were secured in a 4 x 6 rack. The rack was placed into the water bath of the Covaris system containing degassed water at a temperature of $10 \pm 1^{\circ}\text{C}$ and a submerged acoustic transducer. Cell disruption was performed in power tracking mode, automatically by placing each tube in a predetermined sequence in the focal zone of the transducer. A 1% volumetric addition of EDTA stock solution was added after sonication.

A two-level, half-fractional, 5-factorial design with four center points was used to screen for factors significantly contributing to Root Mean Square Error (RMSE). This screening was followed by a two-level, full-fractional, 4-factorial design screening with four center points to study the effect of time at shorter range when biomass concentration was fixed.

Lyticase treatment

MOPS Enzymatic Lysis buffer was heated in a bath to 25°C. Frozen cell paste was resuspended in the warmed buffer to a target biomass value, followed by a 1 hour incubation at 25°C.

Adaptive Focused Acoustics Optimization

After determining significant factors using the half-fractional design described in a previous section, three experiments were performed to generate RSMs to account for (1) vial design and (2) to investigate if performance could be augmented using an enzymatic pre-treatment step described in the previous section. In these three experiments, sonication time as an operating factor was fixed at 60 seconds, as screening beyond this time was shown to have very little effect.

The first experiment used 6mL Chromacol tubes in which 1mL samples were sonicated, the second experiment used the previously mentioned 1mL milliTUBEs in which 1mL samples were sonicated and the third experiment involved the use of 1mL milliTUBEs in which 1mL enzymatically pre-treated samples were sonicated.

For each experiment five RSMs were generated as discussed in the end of the introduction section.

Clarification

Lysates were centrifuged at 4°C and 15000 g for 30 minutes using a benchtop Eppendorf Centrifuge (model 5415R). The supernatant of each sample was filtered with a 0.22µm 33mm Millex PVDF syringe filter (Merck Millipore; Billerica MA, USA). Filtrate was stored at 4-7°C for up to one week until further analysis.

Analytical methods

Screening and Response Surface Methodology

All statistical analysis and model generation was done using JMP®Pro12.0.1 (SAS Institute Incorporation; Cary NC, USA).

Screening models were generated with a minimum resolution of 5 to estimate all possible two-factor interactions. The relative contribution of an individual factor was defined as the total of the sum of squares (Type III) of each factor-associated term as a percentage of the total of the sum of squares of all terms in the screening models. The effects of significant factors on five different responses were studied by generating RSMs. Central Composite Designs (CCDs) with on-face axial points ($\alpha=1$) and two center points were used to generate quadratic RSMs. Only statistically significant model terms ($p<0.05$) were included in each model and were selected using stepwise regression.

Total soluble protein analysis

Total soluble protein analysis of clarified lysates was performed using a Nanodrop 1000 spectrophotometer (Thermo Fisher Scientific; Dartford, UK). Triplicate measurements were performed for 3 μ L sample volumes at an absorbance of 280nm as per manufacturer's instructions.

TC-HBc analysis with immunoblotting

[TC-HBc] analysis was conducted using immunoblotting onto nitrocellulose membranes, using hepatitis B core-specific antibody (mouse) as a primary antibody and horseradish peroxidase-fused, mouse-specific antibody (goat) as a secondary antibody. Details of this procedure are described below.

Clarified samples were diluted in MOPS/EDTA TX100 to achieve total protein concentrations of 1mg/mL at a total volume of 50 μ L in 0.2mL Protein LoBind PCR tubes (Cat. No. 951010022).

Reference standard, Recombinant Hepatitis B Core Antigen, (Abcam; Cat No. AB49013; Cambridge, UK) was diluted in MOPS/EDTA TX100 buffer to achieve 100 μ L stock concentrations of 150 μ g/mL and 100 μ g/mL. These stock solutions were serially diluted two-fold to final volumes of 50 μ L to generate reference curves.

5 μ L 10X NuPage® Sample Reducing Agent was added to all aliquots. These were subsequently heated at 95°C for 10 minutes using a Bio-Rad C1000 Touch™ Thermal Cycler and subsequently cooled for at least 15 minutes at 12°C.

For each assay, a 0.45 μ m 11.5 x 8.5 cm nitrocellulose membrane was placed on a piece of filter paper (12 x 9cm) resting on a table. Using a 12 x 8 roster to serve as a grid, samples were applied on the membrane in 2 μ L volumes. Each membrane was dried for at least 10 minutes at room temperature post sample application.

After drying, the membranes were blocked in 5% skimmed milk power PBS-T (0.05% Tween20) solution for 1 hour at room temperature or overnight at 4-7°C. Hepatitis B virus core antigen-specific, mouse monoclonal antibody (Abcam; Cat. No. AB8639; Cambridge, UK) was applied in a 1:1000 solution in 2.5% Skimmed Milk Power PBS-T and incubated for 45 minutes at room temperature and washed three times for 5 minutes each wash with PBS-T. Secondary antibody (Abcam; Cat. No. A4416-1ML; Cambridge, UK) was applied in a 1:2000 dilution in PBS-T followed by a 30-minute incubation at room temperature. Membranes were finally washed three times for 5 minutes with PBS-T and once for 5 minutes with PBS to rinse away residual detergent. 10mL of Bio-Rad's Clarity Western ECL substrate was used to develop the membranes. Detection was performed using automated exposure setting on an Amersham Imager 600. Dot blot densitometry was done using ImageQuant software followed by quantification with four-parameter logistic (4PL) fitting.

Microscopy

Unclearified lysate samples were diluted to $[X]=5-10\text{g/L}$ using PBS and stained using a 1:1000 volumetric addition of boron-dipyrromethene (BODIPY[®]) in DMSO. After an incubation period of 15 minutes, 5 μL aliquots of stained suspension were used to prepare microscopy slides. Microscopy analysis was done in bright light microscopy and fluorescent imaging modes using a Nikon Eclipse microscope.

Particle Size Distribution Analysis

PSD analysis was performed using a Malvern Mastersizer 3000. Crude, unclarified, lysate was applied to the Hydro SV Dispersion unit at 1000rpm until laser obscuration was in the 5-10% range. 5 measurements of each sample were taken to subsequently create an average PSD curve.

Results and discussion

High Pressure Homogenization Optimization

Figure 3 shows the effect of biomass concentration $[X]$, operating pressure (p) and the number of passes (N) on cell disruption (R) expressed as the total amount of soluble total protein (mg/mL). The response model can be described with the following formula: $R = -6.14 \cdot 10^{-1} N^2 - 8.92 \cdot 10^{-6} p^2 + 1.38 \cdot 10^{-3} Np + 1.97 \cdot 10^{-4} p[X] + 4.20N + 8.4 \cdot 10^{-3} p - 1.00 \cdot 10^{-3} [X] - 5.15$.

As indicated by the term $1.97 \cdot 10^{-4} p[X]$ the factor interaction of biomass concentration and pressure has a positive effect on the level of cell disruption. The term is highly significant ($p=0.00253$) which is in contrast with the assumption made by others¹⁷ that the effect of biomass concentration on cell disruption is minor. This difference is most likely because Follows et al. investigated cell disruption at a significantly higher cell suspension concentration range (450-750g/L vs 50-100g/L) where the effect of biomass had diminished.

Other literature supports the findings of this research that the concentration of biomass has a significant and positive effect on total cell disruption²⁹.

Unlike for pressure, the optimum number of passes seems to stay the same as the biomass concentration is changed. This is not surprising as no term for $[X]N$ exists in the equation.

However, the term $1.38 \cdot 10^{-3} Np$ indicates a positive factor-interaction between the number of passes and pressure, which is expected.

Finally, the two quadratic terms of N^2 and p^2 indicate optima for pressure and the number of passes, however it must be noted that these are quadratic estimates that are only valid within the investigated range. The response surface methodology in this series of experiments only considers linear or quadratic functions, not for instance, asymptotic functions which are very common in biological systems and bioprocesses. Therefore, supposed quadratic optima found at the end of the experimental window, could also indicate asymptotic limits. However, establishing this would require further work and does not change the main output of this study.

It should also be noted that cell disruption (R) is just one measure of performance in the context of cell disruption. As mentioned previously, this paper aims to investigate five different performance criteria as response surfaces. Instead of displaying four additional response models, figure 3 summarizes the factor settings for various performance optima derived from corresponding RSMs.

Looking at figure 3, one can conclude that different operating conditions are required to achieve different maximum performance levels. For instance, maximum pressure (1200 bar) is required to achieve maximum cell disruption (R), however sub-maximal pressure (1000 bar) is preferable for maximum purity (P). Note that in figure 3 biomass is excluded from the performance maxima of the response models for specific product recovery (TC-HBC_s) and

purity (P) as this was found to have insignificant contributions to variance for these specific models ($p > 0.05$).

Adaptive Focused Acoustics Characterization

Table 1 shows the results of the first screening experiment which was a five-factor, half factorial design was used to generate two factor screenings.

Biomass ($[X]$) was found to be the most significant factor for both specific (R_s) and total cell disruption (R). However, the magnitude of the range of $[X]$ may have diminished the significance of other factors and may therefore not be representative.

Time, on the other hand, initially seems to be insignificant relative to other factors which was in contradiction other sources²⁴. This could be because the effect of time had already approached a limit and is not significant within the studied range.

To account for these two points of discussion, another screening was performed. In this four-factor full fractional screening, biomass was fixed at $[X] = 55\text{g/L}$ so responses R and R_s were equal. Additionally, the cycles per burst were found to be insignificant. Therefore, in further experiments this was fixed at 1000 cpb. The time range was changed to lower exposure times as it was hypothesized that longer acoustic exposure times were excessive to achieve disruption and would therefore not show as significant contributing to response variance. The results of this screening are shown in table 2. Following two screening experiments it was found that biomass, duty factor, intensity and acoustic exposure time were significant factors. Increasing acoustic exposure time did not have a significant effect beyond 60s. Hence, this factor was fixed at this value while other significant factors were varied to generate RSMs in optimization experiments.

Adaptive Focused Acoustics Optimization

Figure 4 shows how different types of vials, milliTUBE and Chromacol vials, have different effects on cell disruption performance. The milliTUBE vials consistently outperformed

Chromacol vials for every response. As with homogenization, AFA requires different settings depending on the chosen response maxima. For total cell disruption and specific cell disruption (see figure 4A) maximum performance values of the milliTUBE configuration were found to be slightly higher than that for Chromacol vials. However, the values for maximum product recovery and specific recovery (figure 4B) were significantly higher in the milliTUBE vials in comparison to Chromacol vials. This in turn, shown by figure 4C, results in minimal product purity relative to the milliTUBE configuration since $P=[TC-HBc]/R$. Figure 5, showing RSMs of total cell disruption (R) using milliTUBE and Chromacol vials, explains these differences in overall performance. Although AFA-mediated disruption using the Chromacol vials does influence disruption within a certain range, as proven by significant contribution to variance by the studies factors, it's effect on overall disruption is most likely diminished by other mechanisms such as cell autolysis during fermentation, osmotic shock, mechanical stress or heat lysis during buffer resuspension. This is demonstrated in figure 5 by a relatively flat response model compared to that of the milliTUBE configuration.

The underlying mechanism of these differences relate to total vessel volume, total working volume and additional mechanical stress through the addition of an AFA fiber in the milliTUBE vials. Because the total vessel volume of Chromacol vial is significantly larger than that of a milliTUBE vial, acoustic energy is dispersed over a larger volume resulting in lower levels of disruption. Additionally, the Chromacol vials used a 17% working volume, whereas milliTUBE vials were filled to almost 100%. This difference in relative working volumes was a result of standardizing the experiments to absolute working volumes of 1mL.

Larger relative working volumes lead to more efficient cell disruption processes as acoustic energy is directed less to mixing and forming liquid-air interfaces and more towards cavitation nucleation in the lysis medium. As higher working volumes reduce mixing rates in the sample, the added integrated AFA fiber facilitates the generation of high numbers of

uniformly distributed cavitation bubbles. The simultaneous collapse of these high-energy liquid-gas interfaces results in higher levels of mechanical energy and thus higher levels of cell disruption³⁰.

This study also addressed the implementation of an enzymatic pre-treatment step into a cell disruption process. Several sources report that the enzyme, lyticase, hydrolyses beta-glucans in fungal cell walls, resulting in the transformation of cells into so-called protoplasts³¹⁻³³.

Lacking cell walls, these protoplasts are much more susceptible to mechanical stress. Therefore, cell suspension samples were pre-treated with lyticase to augment subsequent AFA-mediated cell disruption.

Results in figure 4 show that this enzymatic pre-treatment step resulted in significantly higher overall performance in AFA-mediated cell disruption compared to the other small-scale methods lacking this enzymatic treatment step.

Anand *et al.* described how pre-treatment of *Escherichia coli* cells affected the first order disruption rate constant, k , for homogenization³⁴. Li *et al.* subsequently described this rate constant in the context of AFA in the following equation at fixed biomass concentration³⁵:

$$\ln\left(\frac{R_m - R_0}{R_m - R}\right) = kt \quad (4)$$

Where R_m is the total maximum available amount of protein available for release. R_0 is the level of protein release prior AFA-mediated cell disruption and was found to be 4.17mg/mL for untreated cells and 16.90mg/mL for enzymatically pre-treated cells ($[X]=100\text{g/L}$). R is the observed level of disruption and t is the acoustic exposure time fixed at 60s.

We did not obtain the absolute value for R_m experimentally but as our purposes are comparative, R_m was chosen to be the maximum observed level of protein release from homogenization at $[X]=100\text{g/L}$ ($R_m=29.6\text{mg/mL}$).

It was hypothesized that the lyticase pre-treatment step would increase the disruption rate constant due to the weakening of cells. However, because of this, it was difficult to determine

how much of the observed cell disruption was due to non-mechanical lysis, such as osmotic shock, or due to AFA-mediated cell disruption. Using the AFA milliTUBE configuration, we found that the disruption rate constant for AFA-mediated disruption preceded by lyticase treatment ($k_{LY,AFA} = 6.82 \cdot 10^{-3} \text{ s}^{-1}$) was 2.65 times higher than the disruption rate constant of AFA-mediated cell disruption ($k_{AFA} = 2.57 \cdot 10^{-3} \text{ s}^{-1}$). This strongly suggests that enzymatic pre-treatment augments performance of AFA-mediated cell disruption by weakening cells.

Because of this pre-treatment, maximum levels of AFA-mediated cell disruption almost matched maximum levels achievable with HPH. Moreover, the performance of the augmented AFA method for maximum specific product recovery was superior to that of HPH. Likewise, as shown in figure 4C, both platforms using milliTUBEs achieved higher product purity levels than HPH.

Just as HPH requires different operating settings depending on the response studied, AFA optima settings depend on the choice of performance criteria *and* the mode of AFA (figure 4D).

Product recovery

The previous section demonstrated the differences in various response between HPH and various modes of AFA. This section aims to explain the mechanisms involved behind the performance of the discussed cell disruption methods.

Figure 6A shows Particle Size Distribution (PSD) curves of various unclarified lysates from disrupted samples. The amount of micronized debris (less than $1 \mu\text{m}$) generated through HPH is much higher than that generated through AFA-mediated disruption. These high levels of micronized debris are associated with high levels of cell disruption, however also impede recovery of product. This is demonstrated in figure 6B where HPH is shown to lead to lower product purities than AFA despite higher levels of cell disruption.

Interestingly, the enzymatic pre-treatment step did not lead to a significant change in PSD even though it significantly increased levels of cell disruption. This is probably why the maximum purity level of milliTUBE AFA-mediated disruption is comparable to that of milliTUBE AFA-mediated disruption preceded by lyticase treatment.

The generation of micronized debris during HPH (figure 6A) can lead to the subsequent formation of aggregates as seen in figure 7A. The fluorescent BODIPY stain shows neutral lipids in intact cells that were adhered together by cell debris. Such aggregation can severely limit the release of the hydrophilic product into the supernatant upon subsequent clarification.

In contrast, AFA-mediated cell disruption does not seem to generate micro debris. As shown in figure 7B, a cell disrupted by AFA releases its lipid content out of the cell wall without forming large aggregates. Similar results are observed in figure 7C, showing a lyticase treated sample that is subsequently disrupted using AFA (figure 7D).

Process scaling and cell disruption mimicry

So far, this paper has made multiple comparisons between the relatively large-scale industry standard of cell disruption, HPH, and various modes of small-scale, non-contact AFA methods.

For some performance criteria, we have found that it is possible for AFA to outperform HPH.

However, when scaling down a process, the goal is often not to outperform the large-scale surrogate but to mimic its performance as close as possible. To achieve this, one must define these performance criteria.

This study considered a scenario where the objective was to maximize product purity from a homogenization process and, using enzyme-augmented AFA, mimic both the level of purity *and* the corresponding level of product recovery at the same homogenization parameter settings.

First, operating ranges were defined by determining standard deviation windows of (1) maximum product purity, P , and (2) the corresponding level of product recovery, $[TC-HBc]$, at maximum purity of HPH.

Overlaying the purity and product recovery response functions for enzymatically augmented AFA, at the specified ranges, yielded the operating domains for duty factor and intensity settings. The corresponding operating window is displayed in white in figure 8.

It should be noted that the above scenario serves as an example of how the proposed scale-down methods can be implemented to mimic any large-scale cell disruption process. By assigning multiple performance criteria we can achieve more defined conditions to mimic performance at small-scale. Likewise, the same methodology can be applied to scale-up a micro-scale cell disruption process. We therefore believe that the scale-down AFA-mediated cell disruption can be used in a wide array of applications such as high-throughput buffer development and micro-scale fermentation sampling whilst retaining scalable significance.

Conclusions

This paper presents the development of a high-performance, high-throughput small-scale, scalable disruption tool for microbial bioprocess development. This was done by investigating five performance criteria in four modes of cell disruption. One of these modes involved the use of the industry standard of cell disruption, High Pressure Homogenization, and the other three involved various modes of operation of small-scale, non-contact Adaptive Focused Acoustics methods. These investigations were carried out through statistical screening methods, the development of twenty response surface models, various modes of microscopy and particle size distribution analysis.

Significant process parameters for AFA were found to be acoustic exposure time, biomass suspension concentration, duty factor and intensity. After performing optimization experiments for these significant factors, it was found that the design of the vessel in which

samples were sonicated had a great impact on all cell disruption performance criteria. Specifically, it was found that the use milliTUBE vials greatly enhanced performance compared to using Chromacol vials. Performance was subsequently augmented using an enzymatic pre-treatment step. This led to matching and even outperforming homogenization performance, depending on the performance criterion investigated. The resulting overlap of performance ranges between HPH and AFA-mediated cell disruption allowed for small-scale AFA performance mimicry of HPH. Performance mimicry was enhanced by matching multiple performance criteria, as opposed to a single criterion, using overlay plot analysis.

These results demonstrate that AFA-mediated cell disruption could be used as a tool for a wide variety of applications including buffer development, strain selection, fermentation process development and whole bioprocess integration.

Acknowledgements

The authors would like to thank the European Union's Seventh Framework Program for Research and Technological Development (HEALTH-FE-2013-602437) for financial support, iQur limited for technical support and providing the relevant yeast strain; and Alex Ramirez, Michael Whelan and Sushobhan Bandyopadhyay for technical assistance.

Nomenclature

[TC-HBc]: Product concentration / product recovery / Tandem Core Hepatitis B concentration

[X]: Biomass concentration

AFA: Adaptive Focused Acoustics

CER: Carbon Evolution Rate

Cpb: Cycles per Burst

DF: Duty Factor

DoE: Design of Experiments

DOT: Dissolved Oxygen Tension

HPH: High Pressure Homogenization

LY: Lyticase

mTUBE: milliTUBE

P: Product purity

PBS: Phosphate Buffered Saline

PSD: Particle Size Distribution

R: Cell disruption / protein release

RO: Reverse Osmosis

R_s: Specific cell disruption / specific protein release

RSM: Response Surface Methodology or Response Surface Model

RSME: Root Mean Square Error

TC-HBc: Tandem Core Hepatitis B core protein

TC-HBc_s: Specific product recovery

VLP: Virus-Like Particle

WCW: Wet Cell Weight

Literature Cited

1. Bower DM, Lee KS, Ram RJ, Prather KLJ. Fed-batch microbioreactor platform for scale down and analysis of a plasmid DNA production process. *Biotechnol Bioeng.* 2012;109(8):1976-1986. doi:10.1002/bit.24498.
2. Guy HM, McCloskey L, Lye GJ, Mitrophanous K A, Mukhopadhyay TK. Characterization of lentiviral vector production using microwell suspension cultures of HEK293T-derived producer cells. *Hum Gene Ther Methods.* 2013;24(April):125-139. doi:10.1089/hgtb.2012.200.
3. Mukhopadhyay TK, Allison N, Charlton S, et al. Evaluation of anthrax vaccine production by *Bacillus anthracis* Sterne 34F2 in stirred suspension culture using a miniature bioreactor: A useful scale-down tool for studies on fermentations at high containment. *Biochem Eng J.* 2010;50(3):139-144. doi:10.1016/j.bej.2010.03.011.
4. Noyes A, Huffman B, Godavarti R, et al. High throughput screening of particle conditioning operations: I. System design and method development. *Biotechnol Bioeng.* 2015;112(8):1554-1567. doi:10.1002/bit.25575.
5. Ahmad M, Hirz M, Pichler H, Schwab H. Protein expression in *Pichia pastoris*: Recent achievements and perspectives for heterologous protein production. *Appl Microbiol Biotechnol.* 2014;98(12):5301-5317. doi:10.1007/s00253-014-5732-5.
6. Canales M, Enríquez A, Ramos E, et al. Large-scale production in *Pichia pastoris* of the recombinant vaccine GavacTM against cattle tick. *Vaccine.* 1997;15(4):414-422. doi:10.1016/S0264-410X(96)00192-2.
7. Hamilton SR, Gerngross TU. Glycosylation engineering in yeast: the advent of fully humanized yeast. *Curr Opin Biotechnol.* 2007;18(5):387-392. doi:10.1016/j.copbio.2007.09.001.

8. Josefsberg JO, Buckland B. Vaccine process technology. *Biotechnol Bioeng.* 2012;109(6):1443-1460. doi:10.1002/bit.24493.
9. Nett JH, Cook WJ, Chen MT, et al. Characterization of the *Pichia pastoris* Protein-O-mannosyltransferase Gene Family. *PLoS One.* 2013;8(7):1-13. doi:10.1371/journal.pone.0068325.
10. Potgieter TI, Kersey SD, Mallem MR, Nylen AC, D'Anjou M. Antibody expression kinetics in glycoengineered *Pichia Pastoris*. *Biotechnol Bioeng.* 2010;106(6):918-927. doi:10.1002/bit.22756.
11. De Schutter K, Lin Y-C, Tiels P, et al. Supplementary: Genome sequence of the recombinant protein production host *Pichia pastoris*. *Nat Biotechnol.* 2009;27(6):561-566. doi:10.1038/nbt.1544.
12. Wang J, Nguyen V, Glen J, Henderson B, Saul A, Miller LH. Improved yield of recombinant merozoite surface protein 3 (MSP3) from *Pichia pastoris* using chemically defined media. *Biotechnol Bioeng.* 2005;90(7):838-847. doi:10.1002/bit.20491.
13. Cregg JM. Distinctions Between *Pichia pastoris* and Other Expression Systems. *Pichia Protoc.* 2007;389:1-10. doi:10.1007/978-1-59745-456-8_1.
14. Damasceno LM, Huang CJ, Batt CA. Protein secretion in *Pichia pastoris* and advances in protein production. *Appl Microbiol Biotechnol.* 2012;93(1):31-39. doi:10.1007/s00253-011-3654-z.
15. Doran PM. Cell Disruption. In: *Bioprocess Engineering Principles.* ; 2013:467.
16. Middelberg APJ. Microbial Cell Disruption by High-Pressure Homogenization. *Downstr Process Proteins Methods Protoc.* 2000;9:11-22.
17. Follows M, Hetherington PJ, Dunnill P, Lilly MD. Release of enzymes from bakers'

- yeast by disruption in an industrial homogenizer. *Biotechnol Bioeng*. 1971;13(4):549-560. doi:10.1002/bit.260130408.
18. Kleinig AR, Mansell CJ, Nguyen QD, Badalyan A, Middelberg APJ. Influence of broth dilution on the disruption of *Escherichia coli*. *Biotechnol Tech*. 1995;9(10):759-762. doi:10.1007/BF00159244.
19. Jennings V, Lippacher A, Gohla SH. Medium scale production of solid lipid nanoparticles (SLN) by high pressure homogenization. *J Microencapsul*. 2002;19(1):1-10. doi:10.1080/713817583.
20. Kensy F, Engelbrecht C, Büchs J. Scale-up from microtiter plate to laboratory fermenter: evaluation by online monitoring techniques of growth and protein expression in *Escherichia coli* and *Hansenula polymorpha* fermentations. *Microb Cell Fact*. 2009;8:68. doi:10.1186/1475-2859-8-68.
21. Slinsby F, Dewar S. *Use of the Ambr® 250 in Combination with High-Throughput Design and Analysis Tools for Rapid, Scalable USP Development.*; 2015.
22. von der Haar T. Optimized protein extraction for quantitative proteomics of yeasts. *PLoS One*. 2007;2. doi:10.1371/journal.pone.0001078.
23. Ludlow CL, Scott AC, Cromie GA, et al. High-throughput Tetrad Analysis. *Nat Methods*. 2014;10(7):1-16. doi:10.1038/nmeth.2479.High-throughput.
24. Wenger MD, DePhillips P, Bracewell DG, University College London, Merck & Co. A microscale yeast cell disruption technique for integrated process development strategies. *Biotechnol Prog*. 2008;24(3):606-614. doi:10.1021/bp070359s.
25. Covaris. E-series User manual. 2011. http://covarisinc.com/wp-content/uploads/pn_010041.pdf.
26. Holmes K, Shepherd DA, Ashcroft AE, Whelan M, Rowlands DJ, Stonehouse NJ.

- Accepted Article
- Assembly pathway of hepatitis B core virus-like particles from genetically fused dimers. *J Biol Chem*. 2015;290(26):16238-16245. doi:10.1074/jbc.M114.622035.
27. Invitrogen Corporation. *Pichia* Fermentation Process Guidelines Overview Overview , continued. 2002:1-11.
https://tools.thermofisher.com/content/sfs/manuals/pichiaferm_prot.pdf.
28. Rodriguez E. Heavy Labeling of Recombinant Proteins. In: *Pichia Protocols*. ; 2007:159.
29. Patil MD, Patel G, Surywanshi B, Shaikh N, Garg P, Chisti Y. Disruption of *Pseudomonas putida* by high pressure homogenization: a comparison of the predictive capacity of three process models for the efficient release of arginine deiminase. *AMB Express*. 2016;6:84. doi:10.1186/s13568-016-0260-6.
30. Covaris Inc. Covaris Product catalogue: microTUBE.
<http://covarising.com/products/afa-tubes-and-vials/microtube/>. Published 2017.
Accessed January 1, 2017.
31. Burden D. Zymolyase™ vs Lyticase and Glusulase.
http://www.amsbio.com/brochures/Zymolyase_Comparison.pdf.
32. Miyajima Y, Satoh K, Umeda Y, Makimura K. Quantitation of fungal DNA contamination in commercial Zymolyase and Lyticase used in the preparation of fungi. *Japanese J Med Mycol*. 2009;50(4):259-262. doi:10.3314/jjmm.50.259.
33. Salazar O, Asenjo JA. Enzymatic lysis of microbial cells. *Biotechnol Lett*. 2007;29(7):985-994. doi:10.1007/s10529-007-9345-2.
34. Anand H, Balasundaram B, Pandit AB, Harrison STL. The effect of chemical pretreatment combined with mechanical disruption on the extent of disruption and release of intracellular protein from *E. coli*. *Biochem Eng J*. 2007;35(2):166-173. doi:10.1016/j.bej.2007.01.011.

35. Li Q, Aucamp JP, Tang A, Chatel A, Hoare M. Use of focused acoustics for cell disruption to provide ultra scale-down insights of microbial homogenization and its bioprocess impact-recovery of antibody fragments from rec *E. coli*. *Biotechnol Bioeng.* 2012;109(8):2059-2069. doi:10.1002/bit.24484.

Accepted Article

Tables

Table 1: Relative factor contributions in a five factor, two-level, half fractional factorial screening designs

Factor	DF (%)	cpb	I (mv)	t (s)	[X] (g/L)	
<i>Range</i>	<i>(0.1,20)</i>	<i>(50,1000)</i>	<i>(0.1,10)</i>	<i>(60,300)</i>	<i>(10,100)</i>	
% contribution	Total disruption (R)	23.5%	8.6%	9.9%	8.7%	49.1%
	Specific disruption (R_s)	1.6%	0.1%	0.3%	0.3%	97.7%

Two different screenings were performed: One for R and one for R_s .

Table 2: Relative factor contributions in a four-factor, two-level, full-fractional factorial screening design

Factor	DF (%)	cpb	I (mv)	t (s)	
<i>Range</i>	<i>(0.1,20)</i>	<i>(50,1000)</i>	<i>(0.1,10)</i>	<i>(10,60)</i>	
% contribution	Total cell disruption (R=R_s)	40.1%	0.4%	38.4%	21.1%

Figures

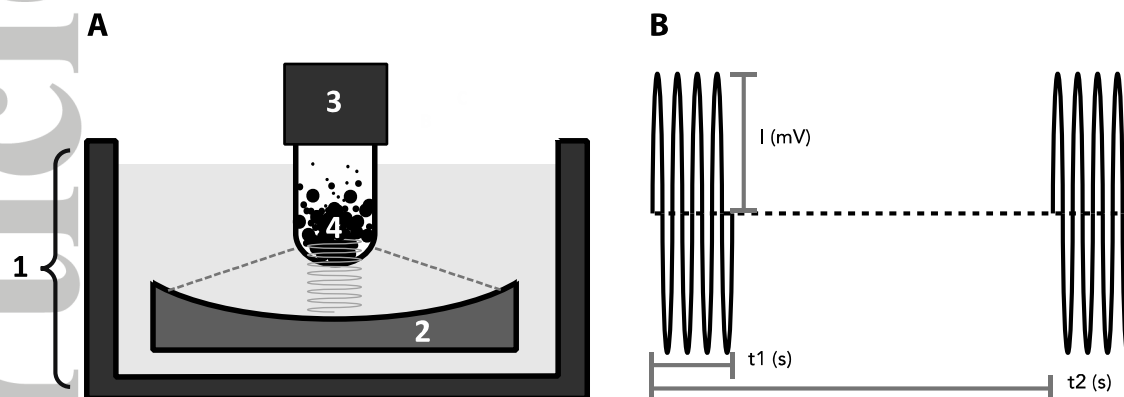


Figure 1: **Covaris components and parameters.** (A1) Tank containing cooled degassed deionized water, (A2) acoustic transducer, (A3) vial containing suspended cells and (A4) acoustic focal zone. (B) Covaris parameters: Duty Factor, DF (%), refers to the relative time between sonic bursts, hence $DF = (t_1/t_2) \cdot 100\%$. Intensity, I (mV), denotes the amplitude of the sonic wave. Cycles per burst, cpb , refers to the amount of cycles per acoustic wave. In this case, cpb is 4. Time, t (s), simply refers to the total time a sample is exposed to sonication treatment. $[X]$ (g/L) refers to the wet cell biomass concentration in suspension.

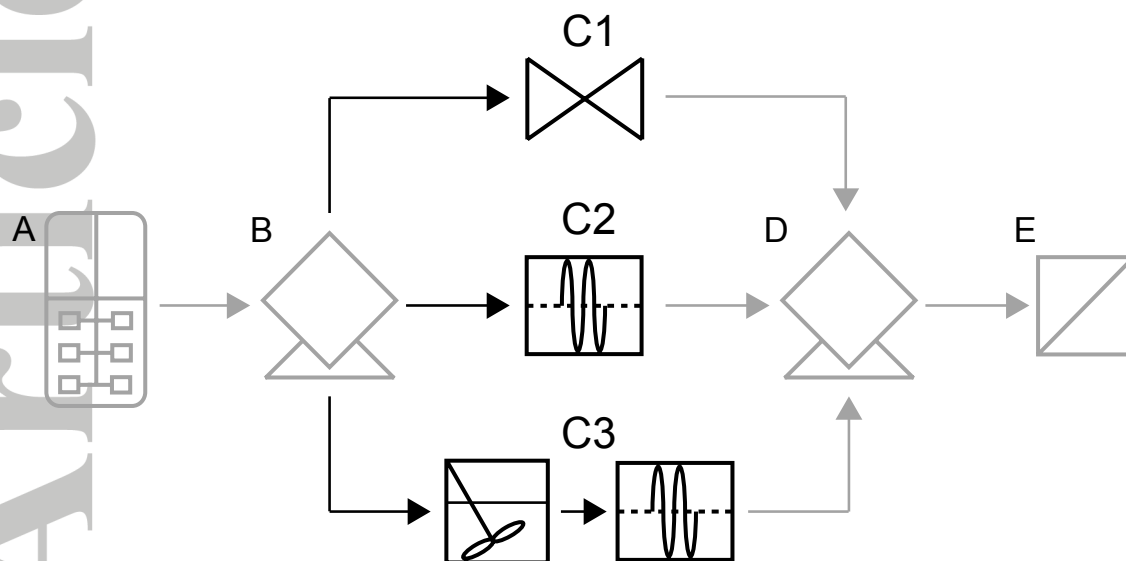


Figure 2: **Process overview of experimental methods.** (A) *P.pastoris* fermentation. (B) Harvest centrifugation at 3000 g, 20 min, 4°C. (C1) HPH of resuspended pellet at $T=8\pm 2^{\circ}\text{C}$ and variable p , N and $[X]$. (C2) AFA of resuspended pellet at $T=9\pm 1^{\circ}\text{C}$ and variable I , DF , cpb and t using either 1mL milliTUBE vials or 6mL Chromacol vials. (C3) Lyticase pre-treatment of resuspended pellet (25°C, 1h) followed by AFA at $T=9\pm 1^{\circ}\text{C}$ and variable I , DF , cpb and t using 1mL milliTUBE vials. (D) Clarification centrifugation of crude lysate at 15000 g, 30min, 4°C. (E) Dead-end filtration (0.22μm) of supernatant.

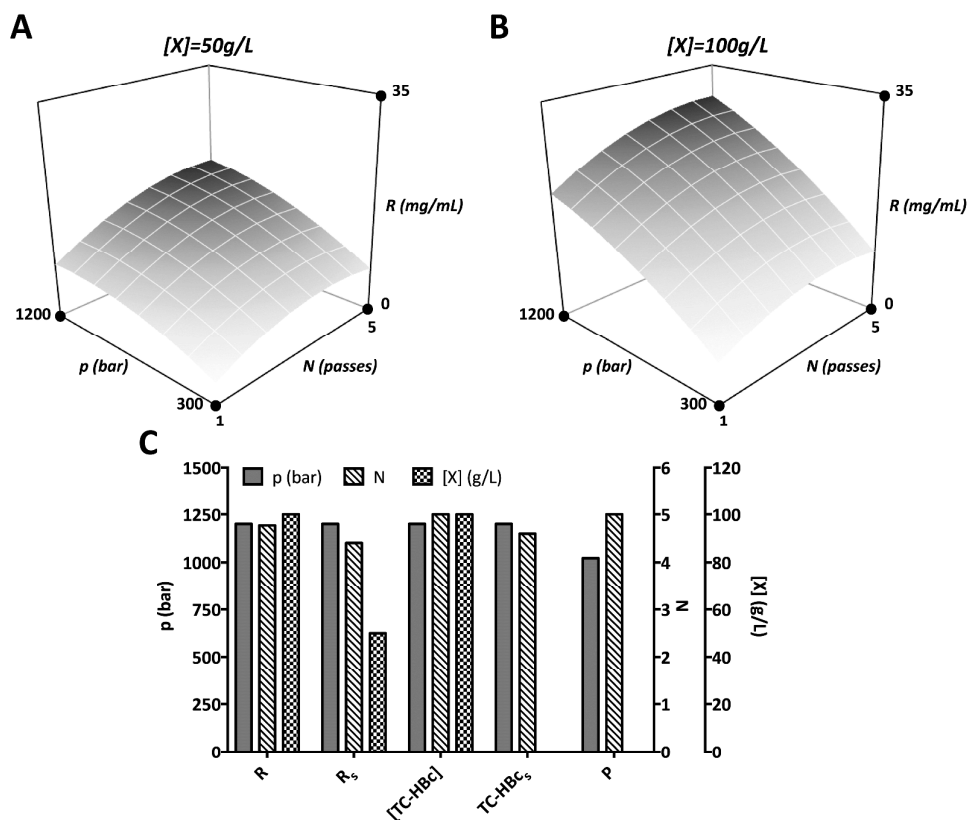


Figure 3: **High Pressure Homogenization performance.** (A and B) Response Surface Models at different level of $[X]$ for total cell disruption measured as total soluble protein, R (mg/mL). (C) Factor values and optima for various responses: R ($r^2=0.98$), R_S ($r^2=0.97$), $[TC-HBc]$ ($r^2=0.92$), $TC-HBc_S$ ($r^2=0.90$) and P ($r^2=0.77$).

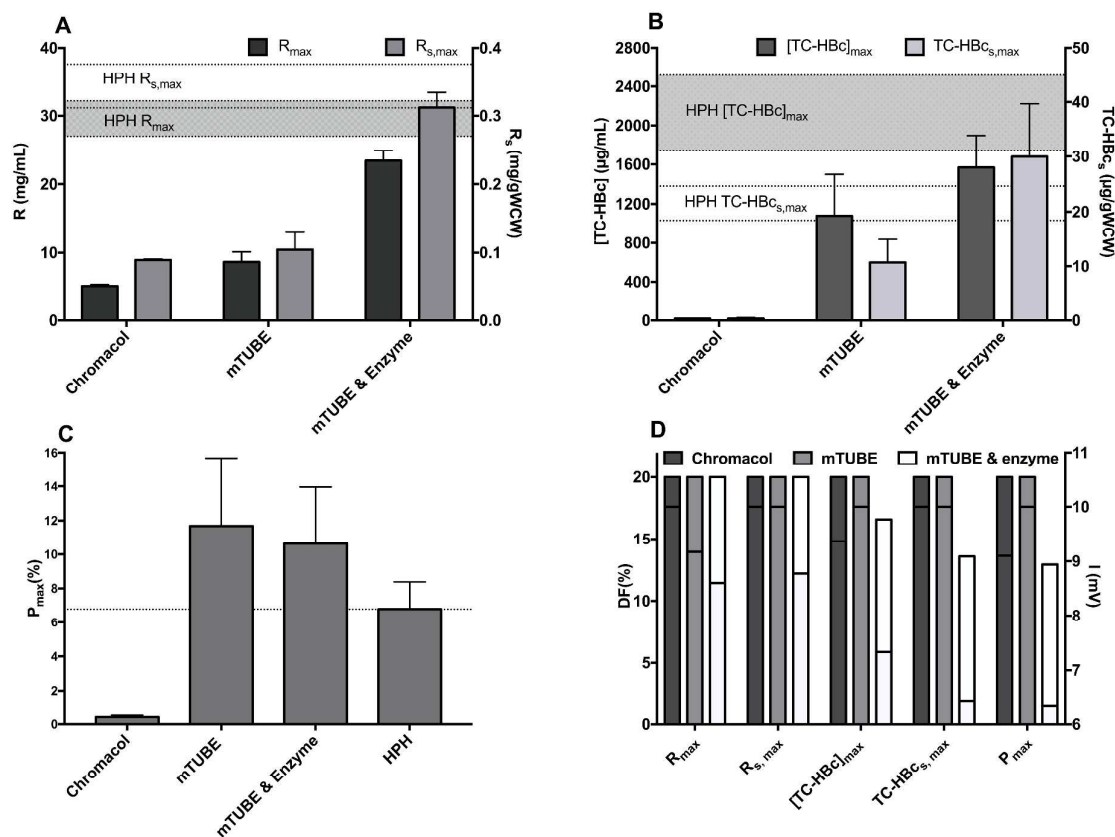


Figure 4: **Summary of Response Surface Models for Adaptive Focused Acoustic methods.** (A-C) Maximum response ranges for various performance criteria. (A) On the left y-axis, the level of total cell disruption (R); on the right y-axis, the specific level of cell disruption (R_s). (B) On the left y-axis the level of total product recovery ($[TC-HBc]$); on the right y-axis, the specific level of product recovery ($TC-HBc_s$). (A, B) The horizontal grid lines display the maximum model ranges of the studied responses of High Pressure Homogenization (HPH). (C) Purity (P) performance ranges. (D) Different factor values to achieve optima. Intensity values are superimposed over duty factor values.

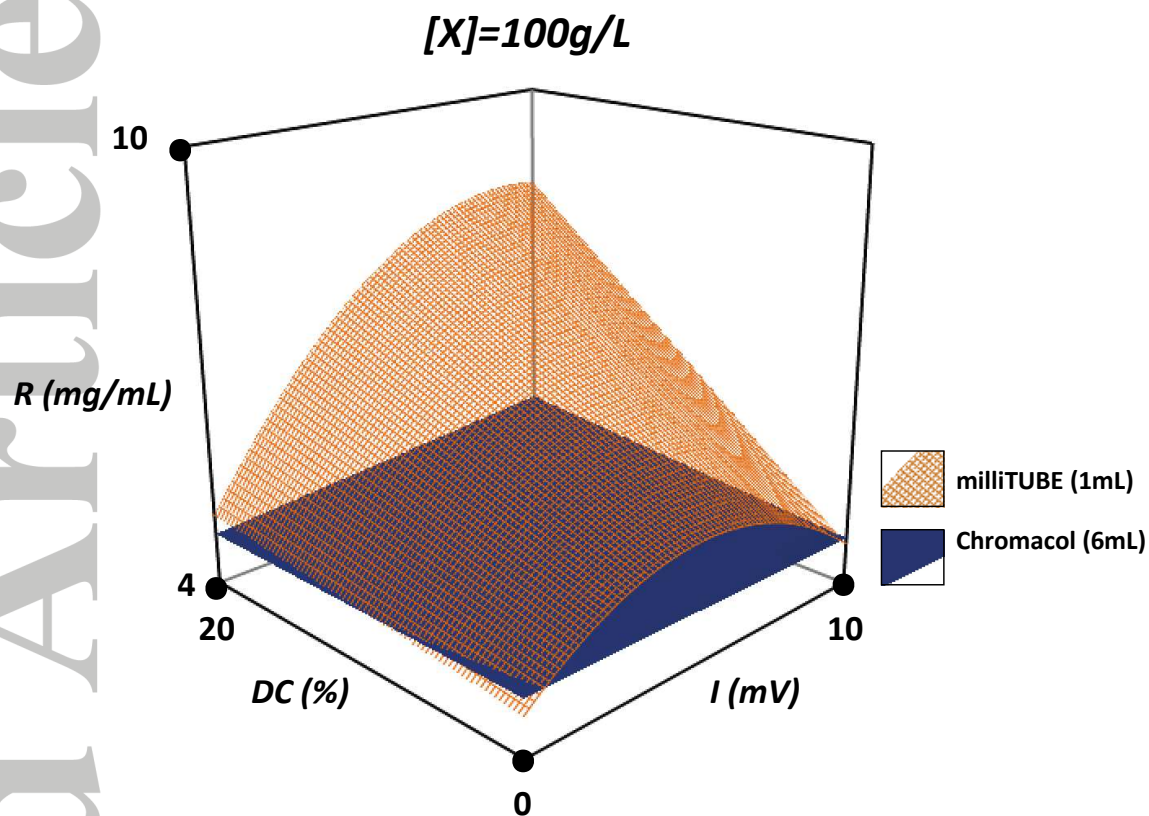


Figure 5: **Effect of vial design.** Response Surface Models at $[X]=100\text{g/L}$ WCW and $t=60\text{s}$ for two configurations of AFA-mediated cell disruption. (1) Using 6mL Chromacol vials: (2) 1mL milliTUBE vials with integrated acoustic fibres.

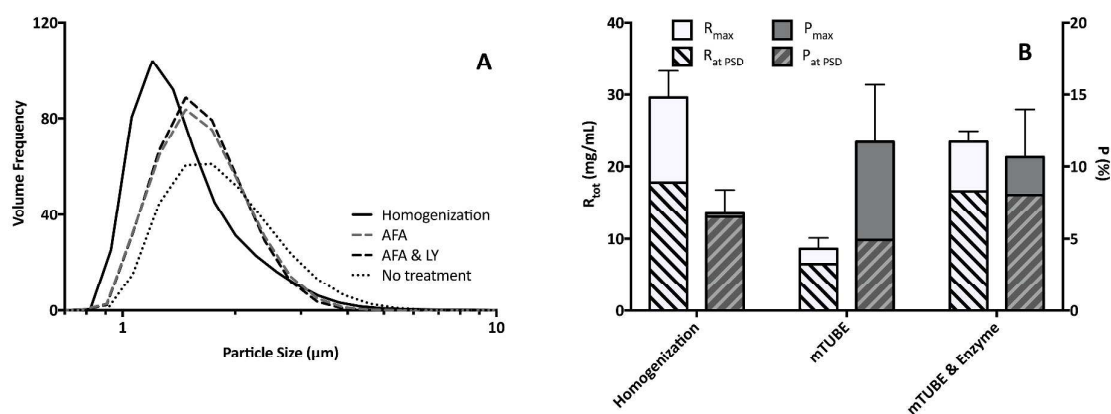


Figure 6: **Effect of micronized debris on purity.** (A) PSD analysis of untreated cells in suspension ($[X]=50\text{g/L}$) and respective crude lysates disrupted by homogenization ($p=1200$ bar, $N=5$ passes, $T=8\pm 2^\circ\text{C}$), AFA ($I=10\text{mV}$, $DF=20\%$, $cpb=1000$, $t=60\text{s}$, $T=9\pm 1^\circ\text{C}$) and AFA preceded by lyticase incubation ($t=1\text{hr}$, $T=25^\circ\text{C}$). (B) Modelled quantitative analysis of clarified lysates disrupted by AFA, AFA preceded by lyticase incubation and homogenization. Two levels of cell disruption (R) and product purity (P) are given: the maximum values of the respective Response Surface Models (R_{max} , P_{max}) and, superimposed, the levels of disruption and purity ($R_{\text{at PSD}}$, $P_{\text{at PSD}}$) achieved at the same disruption conditions represented by the PSD curves. Error bars correspond to performance maxima only.

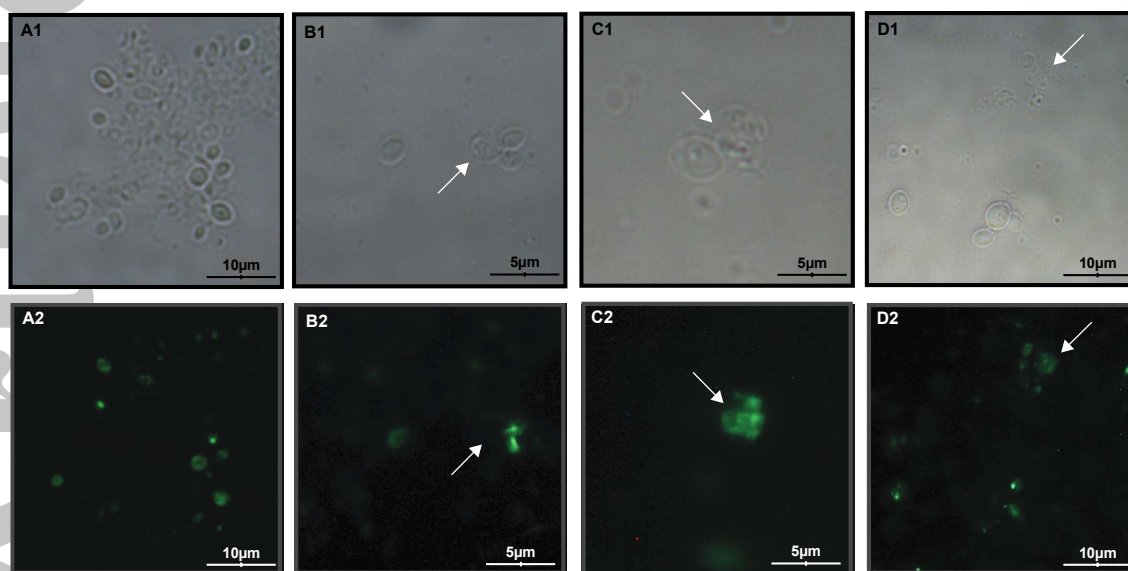


Figure 7: **Impact of cell disruption method on cell debris and aggregation.** Microscopy images of lysates ($[X]=50\text{g/L}$) at 101.5x magnification. (A1) Bright light microscopy image of homogenized sample ($p=1200$ bar, $N=5$ passes, $T=8\pm 2^\circ\text{C}$) and (A2) corresponding fluorescent image showing lipid content. (B1, B2) AFA ($I=10\text{mV}$, $DF=20\%$, $cpb=1000$, $t=60\text{s}$, $T=9\pm 1^\circ\text{C}$). (C1, C2) Lyticase pretreated sample. (D1, D2) Lyticase pretreated sample followed by AFA mediated disruption ($I=10\text{mV}$, $DF=20\%$, $cpb=1000$, $t=60\text{s}$, $T=9\pm 1^\circ\text{C}$).

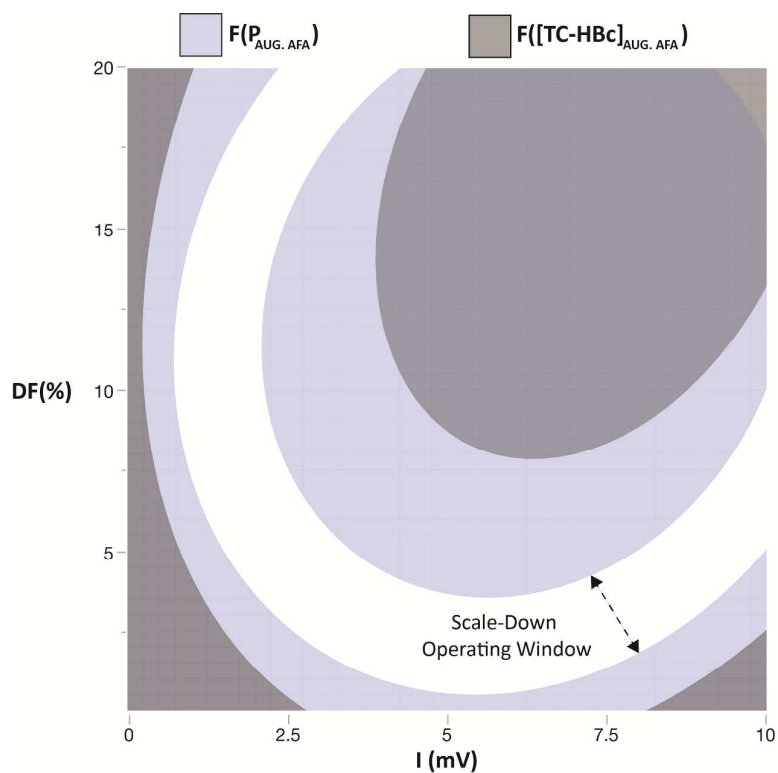


Figure 8: **Microscale process mimicry.** Overlay plot of enzymatically augmented AFA-mediated cell disruption functions of purity, $F(P_{AUG.AFA})$, and product recovery, $F([TC-HBc]_{AUG.AFA})$ at $[X]=50$ g/L and $t=60$ s.